# Gas-Phase Activation and Reaction Dynamics of Chiral Ion–Dipole Complexes

**Antonello Filippi and Maurizio Speranza*[a]**

**Abstract:** A family of enantiomerically pure oxonium ions, that is O-protonated 1-aryl-1-methoxyethanes, has been generated in the gas phase by the $(CH_3)_2Cl^+$ methylation of the corresponding 1-arylethanols. Some information on their reaction dynamics was obtained from a detailed kinetic study of their inversion of configuration and dissociation. The activation parameters of the inversion reaction are found to obey two different isokinetic relationships depending upon the nature and the position of the substituents in the oxonium ions. In contrast, the activation parameters of the dissociation reaction obey a single isokinetic relationship. The inversion and dissociation rate constants do not follow simple linear free-energy relationships. This complicated kinetic picture has been rationalized in terms of different activation dynamics in gaseous $CH_3Cl$, which, in turn, determine the reaction dynamics of the oxonium ion. When the predominant activation of the oxonium ion involves resonant energy exchange from the 1015 $cm^{-1}$ $CH_3$ rocking mode of unperturbed $CH_3Cl$, the inversion reaction proceeds through the dynamically most favored TS, characterized by the unassisted $C_\alpha$–O bond elongation. When, instead, the activation of the oxonium ions requires the formation of an intimate encounter complex with $CH_3Cl$, the inversion reaction takes place via the energetically most favored TS, characterized by multiple coordination of the $CH_3OH$ moiety with the $H_\alpha$ and $H_{ortho}$ atoms of the benzylic residue. The activation dynamics operating in the intimate encounter complex with $CH_3Cl$ is also responsible for the dissociation of most selected oxonium ions.

**Keywords:** gas-phase activation · ion–molecule reactions · ion–dipole complexes · kinetics · reaction dynamics

## Introduction

Knowledge of the dynamics of ion–dipole intermediates involved in ionic reactions represents a crucial step towards the unequivocal comprehension of the detailed mechanism of such reactions.[1] Recently, ion–dipole dynamics have been probed by fast kinetic methods, but the rate constant for reorganization of ion–dipole pairs in the condensed phase remains essentially unknown. The presence of a nucleophilic solvent represents a major obstacle, which often affects the kinetics and the mechanisms of ionic processes. This interference is obviously unavoidable in solvolytic reactions, such as the acid-catalyzed solvolysis of optically active 1-phenylalkanols and their methyl ethers.[2, 3] Kinetic investigations of these reactions are based on the competition between the loss of optical activity of the chiral substrate and the exchange of the leaving moiety (YOH in Scheme 1) with a molecule of solvent (for simplicity, the solvent cage is represented by $H_2O$ in Scheme 1).

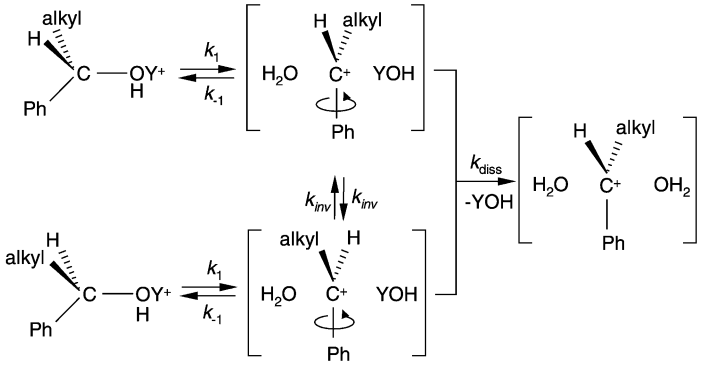


Scheme 1.

The effects of the nucleophilic solvent cage was recently identified by investigating the "solvolysis" of optically active 1-phenylethanol and its methyl ethers in the gas phase.[4] The absence of the solvent and the possibility of modulating the concentration of the added nucleophiles in the gas phase

[a] Prof. M. Speranza, Dr. A. Filippi
Dipartimento di Studi di Chimica e Tecnologia delle Sostanze Biologicamente Attive (No 64)
Facoltà di Farmacia
Università degli Studi di Roma "La Sapienza"
P.le A. Moro 5, 00185 Roma (Italy)
Fax: (+39) 06 49913602
E-mail: maurizio.speranza@uniroma1.it

Supporting information for this article is available on the WWW under http://www.chemeurj.org or from the author.



DOI: 10.1002/chem.200304850

allow us to assess $k_{inv}$ versus $k_{diss}$ without any perturbation from the reaction medium and incursion of spurious bimolecular substitution and elimination–addition pathways.

The investigation is now extended to differently substituted 1-arylethanols. The aim is to elucidate the *intrinsic* dynamics of their acid-catalyzed inversion of configuration and dissociation reactions in the absence of cooperating and perturbing effects of both the solvent and the counterion.

Chiral oxonium ions $\mathbf{I_S}-\mathbf{IV_S}$ are conveniently produced in the gas phase by methylating the corresponding optically active 1-(X-phenyl)ethanols (X = *para*-$CH_3$ (**1$_S$**), *para*-Cl (**2$_S$**), *meta*-$CF_3$ (**3$_S$**), *para*-$CF_3$ (**4$_S$**)) with $(CH_3)_2Cl^+$ ions (Scheme 2). In the same way, the oxonium ions $\mathbf{V_R}$ and $\mathbf{VI_R}$ were obtained in the gas phase from pure *(R)*-(+)-1-(pentafluorophenyl)ethanol (**5$_R$**) and (*R*)-(−)-α-(trifluoromethyl)benzyl alcohol (**6$_R$**) by attack of the $(CH_3)_2Cl^+$ ions (Scheme 2). These latter ions are generated by γ-radiolysis of $CH_3Cl$, present as the bulk component (720 Torr) of gaseous mixtures containing traces of the alcoholic substrate, $H_2{}^{18}O$, a radical scavenger (i.e. $O_2$), and a powerful base (i.e. $(C_2H_5)_3N$). This procedure allows the formation of $\mathbf{I_S}-\mathbf{IV_S}$ and $\mathbf{V_R}-\mathbf{VI_R}$ in a gaseous, chemically inert medium ($CH_3Cl$) at pressures high enough to ensure their complete thermalization.

**Abstract in Italian:** *Una famiglia di ioni ossonio enantiomericamente puri, i. e. gli ioni 1-aril-1-metossietano protonati all'ossigeno, sono stati generati in fase gassosa per metilazione dei corrispondenti 1-ariletanoli mediante ioni $(CH_3)_2Cl^+$. Alcune informazioni sulla loro dinamica di reazione si sono potute ottenere mediante uno studio cinetico della loro inversione di configurazione e della loro dissociazione. I parametri di attivazione per la reazione di inversione obbediscono a due diverse relazioni isocinetiche che dipendono dalla natura e dalla posizione dei sostituenti negli ioni ossonio. Invece, i parametri di attivazione per la reazione di dissociazione seguono una sola relazione isocinetica. Le costanti cinetiche dei processi di inversione e dissociazione non seguono nessuna semplice correlazione lineare di energia libera. Il comportamento cinetico degli ioni ossonio in fase gassosa è stato razionalizzato in termini di differenti dinamiche di attivazione le quali determinano differenti dinamiche di reazione degli ioni stessi. Quando il processo di attivazione dominante in $CH_3Cl$ gassoso procede attraverso uno scambio di energia vibrazionale risonante fra lo ione ed l'oscillazione a 1015 $cm^{-1}$ del metile di una molecola non perturbata di $CH_3Cl$, la reazione di inversione dell'ossonio procede attraverso lo stato di transizione dinamicamente favorito, caratterizzato dalla elongazione non assistita del legame $C_\alpha$-O. Quando, invece, l'attivazione dello ione ossonio richiede la formazione di un complesso di collisione intimamente legato con una molecola di $CH_3Cl$, la reazione di inversione procede attraverso lo stato di transizione energeticamente favorito, caratterizzato dalla coordinazione multipla del gruppo $CH_3OH$ migrante con i centri $H_\alpha$ e $H_{orto}$ del residuo benzilico. La dinamica di attivazione che prevale nel complesso di collisione intimamente legato con una molecola di $CH_3Cl$ governa anche la dinamica di dissociazione degli ioni ossonio considerati.*

## Experimental Section

**Materials**: Methyl chloride and oxygen were high-purity gases from UCAR Specialty Gases N. V., used without further purification. $H_2{}^{18}O$ ($^{18}O$-content > 97%) and $(C_2H_5)_3N$ were purchased from ICON Services. Ring monosubstituted X-styrenes (X = *para*-$CH_3$ (**14**), *para*-Cl (**15**), *meta*-$CF_3$ (**16**), *para*-$CF_3$ (**17**), 2,3,4,5,6-pentafluorostyrene (**18**)) (Scheme 2) were obtained from Aldrich Co. The racemates of 1-(X-phenyl)ethanols (X = *para*-Cl (***rac*-2**), *meta*-$CF_3$ (***rac*-3**), *para*-$CF_3$ (***rac*-4**)), the pure (*R*)- (**5$_R$**) and (*S*)-enantiomers of 1-(pentafluorophenyl)ethanol (**5$_S$**), and the pure *R* (**6$_R$**) and S enantiomers of α-(trifluoromethyl)benzyl alcohol (**6$_S$**) (Scheme 2) were purchased from Aldrich Co. The racemate of 1-(*para*-tolyl)ethanol (*rac*-**1**) was supplied by Lancaster Co. The *S* enantiomers of 1-(X-phenyl)ethanols (X = *para*-$CH_3$ (**1$_S$**), *para*-Cl (**2$_S$**), *meta*-$CF_3$ (**3$_S$**), *para*-$CF_3$ (**4$_S$**)), used as starting substrates, were purified from the corresponding racemates by enantioselective semipreparative HPLC on the following chiral columns: *i*: **1$_S$**: FSC-poly-DACH-METACR, 5 μm, 250 × 4.0 mm i.d., eluent: 70/30/5 (v/v/v) *n*-hexane/dichloromethane/1,4-dioxane; flow rate: 1.0 mL min$^{-1}$; detection by UV (254 nm) and ORD (polarimeter) in series; [$k_1'(-) = 2.63$; $\alpha = 1.12$; *T*: 25 °C]; *ii*: **2$_S$**: (*R*,*R*)-Ulmo, 5 μm, 250 × 4.0 mm i.d., eluent: 99/1 (v/v) *n*-hexane/propan-2-ol; flow rate: 2.0 mL min$^{-1}$; detection by UV (254 nm) and ORD (polarimeter) in series; [$k_1'(-) = 3.85$; $\alpha = 1.22$; *T*: 25 °C]; *iii*: **3$_S$**: (*R*,*R*)-Ulmo, 5 μm, 250 × 4.0 mm i.d., eluent: 90/10/3 (v/v/v) *n*-hexane/dichloromethane/1,4-dioxane; flow rate: 1.5 mL min$^{-1}$; detection by UV (254 nm) and ORD (polarimeter) in series; [$k_1'(-) = 2.33$; $\alpha = 1.09$; *T*: 25 °C]; *iv*: **4$_S$**: FSC-poly-DACH-METACR, 5 μm, 250× 4.0 mm i.d., eluent: 80/20/3 (v/v/v) *n*-hexane/dichloromethane/1,4-dioxane; flow rate: 1.0 mL min$^{-1}$; detection by UV (254 nm) and ORD (polarimeter) in series; [$k_1'(-) = 4.79$; $\alpha = 1.16$; *T*: 25 °C]. The enantiomeric purity of the isolated enantiomers was checked by enantioselective HRGC on: *i*: MEGADEX DACTBS-β (30% 2,3-di-O-acetyl-6-O-*tert*-butyldimethylsilyl-β-cyclodextrin in OV 1701; 25 m long, 0.25 mm i.d., $d_f$ : 0.25μ) fused silica column, at 60 < T < 170 °C, 4 °C min$^{-1}$; *ii*-MEGADEX 5 (30% 2,3-di-*O*-methyl-6-*O*-pentyl-β-cyclodextrin in OV 1701; 25 m long, 0.25 mm i.d., $d_f$ : 0.25μ) fused silica column at *T* = 125 °C. The *S* and *R* enantiomers of 1-(X-phenyl)-1-methoxyethanes (*S*/*R*: X = *para*-$CH_3$ (**7$_S$**/**7$_R$**), *para*-Cl (**8$_S$**/**8$_R$**), *meta*-$CF_3$ (**9$_S$**/**9$_R$**), *para*-$CF_3$ (**10$_S$**/**10$_R$**)), of 1-(pentafluorophenyl)-1-methoxyethane (**11$_S$**/**11$_R$**), and of 1-(α-(trifluoromethylphenyl)-1-methoxyethane (**12$_S$**/**12$_R$**) were synthesized from the corresponding alcohols by the dimethyl sulfate method.[5] Their identities were verified by classical spectroscopic methods.

**Procedure**: The gaseous mixtures were prepared by conventional techniques by using a greaseless vacuum line. Either the *S* enantiomer of the selected 1-(X-phenyl)ethanols (**1$_S$**–**4$_S$**:0.2–0.6 Torr) or the *R* enantiomers of 1-(pentafluorophenyl)ethanol (**5$_R$**:0.6–1.0 Torr) and α-(trifluoromethyl)benzyl alcohol (**6$_R$**:0.4 Torr), $H_2{}^{18}O$ (2–3 Torr), the radical scavenger $O_2$ (4 Torr), and the powerful base B = $(C_2H_5)_3N$ (0.2–1.2 Torr; proton affinity (PA) = 234.7 kcal mol$^{-1}$)[6] were introduced into carefully degassed 130 mL Pyrex bulbs, each equipped with a break-seal tip. The bulbs were filled with $CH_3Cl$ (720 Torr), cooled to liquid-nitrogen temperature, and sealed off. The irradiation experiments were carried out at constant temperatures ranging from 25 to 160 °C with a $^{60}Co$ source, to a dose of $2 \times 10^4$ Gy at a rate of $1 \times 10^4$ Gy h$^{-1}$, as determined by a neopentane dosimeter. Control experiments, carried out at doses ranging from $1 \times 10^4$ to $1 \times 10^5$ Gy, showed that the relative yields of products are largely independent of the dose. The radiolytic products were analyzed by enantioselective HRGC, with a Perkin-Elmer 8700 gas chromatograph equipped with a flame ionization detector, on the same columns used to analyze the starting alcohols. The products were identified by comparison of their retention volumes with those of authentic standard compounds. Their identities were confirmed by HRGC–MS, using a Hewlett-Packard 5890 A gas chromatograph in line with a HP 5970 B mass spectrometer. Yields were determined from the areas of the corresponding eluted peaks, using the internal standard (i.e. benzyl alcohol) method and individual calibration factors to correct for the detector response. Blank experiments were carried out to exclude the occurrence of thermal decomposition and racemization of the starting alcohols, as well as of their methylated ethers, within the temperature range investigated.

The extent of $^{18}O$ incorporation into the radiolytic products was determined by HRGC-MS, setting the mass analyzer in the selected ion mode (SIM). The ion fragments corresponding to $^{16}O$-[*M* − $CH_3$]$^+$ and $^{18}O$-[*M* −

  

| a | | H | | | $CH_3$ | H | H |
|---|---|---|---|---|---|---|---|
| b | | $CH_3$ | | | H | $CF_3$ | $CH_3$ |
| aryl | 4-$CH_3$-$C_6H_4$ | 4-Cl-$C_6H_4$ | 3-$CF_3$-$C_6H_4$ | 4-$CF_3$-$C_6H_4$ | 2,3,4,5,6-$C_6F_5$ | $C_6H_5$ | $C_6H_5$ |
| *Symbol* | | | | | | | |
| **A** | $\mathbf{1_S}$ | $\mathbf{2_S}$ | $\mathbf{3_S}$ | $\mathbf{4_S}$ | $\mathbf{5_R}$ | $\mathbf{6_R}$ | $\mathbf{7_R}$ |
| $\mathbf{B_{ret}}$ | $\mathbf{I_S}$ | $\mathbf{II_S}$ | $\mathbf{III_S}$ | $\mathbf{IV_S}$ | $\mathbf{V_R}$ | $\mathbf{VI_R}$ | $\mathbf{VII_R}$ |
| $\mathbf{B_{inv}}$ | $\mathbf{I_R}$ | $\mathbf{II_R}$ | $\mathbf{III_R}$ | $\mathbf{IV_R}$ | $\mathbf{V_S}$ | $\mathbf{VI_S}$ | $\mathbf{VII_S}$ |
| $\mathbf{C_{ret}}$ | $\mathbf{7_S}$ | $\mathbf{8_S}$ | $\mathbf{9_S}$ | $\mathbf{10_S}$ | $\mathbf{11_R}$ | $\mathbf{12_R}$ | $\mathbf{13_R}$ |
| $\mathbf{C_{inv}}$ | $\mathbf{7_R}$ | $\mathbf{8_R}$ | $\mathbf{9_R}$ | $\mathbf{10_R}$ | $\mathbf{11_S}$ | $\mathbf{12_S}$ | $\mathbf{13_S}$ |
| $\mathbf{A_{rac}}$ | *rac*-**1** | *rac*-**2** | *rac*-**3** | *rac*-**4** | *rac*-**5** | *rac*-**6** | *rac*-**7** |
| **D** | **14** | **15** | **16** | **17** | **18** | **19** | **20** |

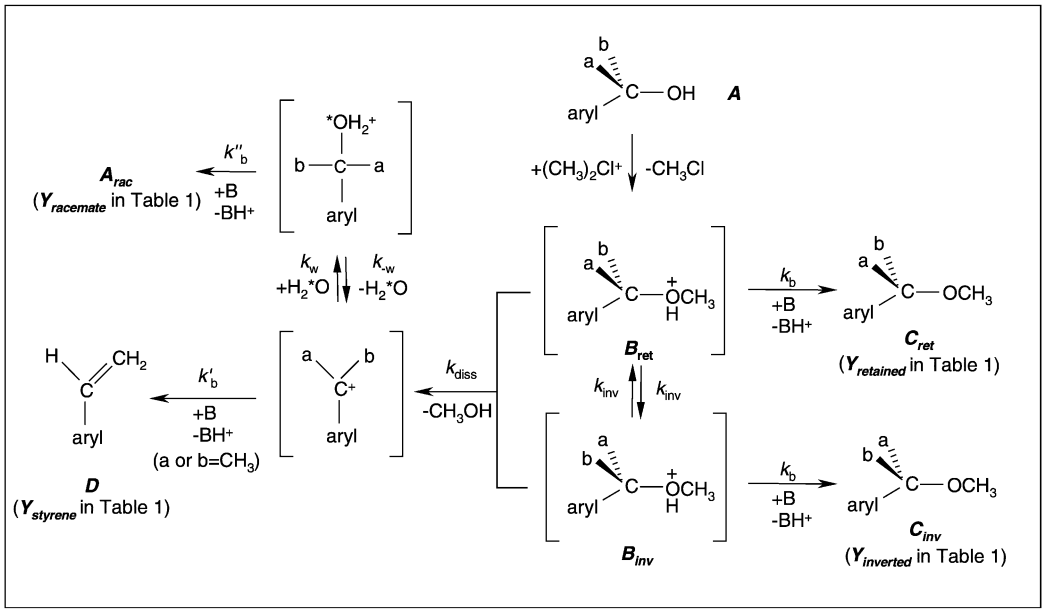


Scheme 2.

$CH_3]^+$ ($M^+$ = parent ion) were monitored to analyze alcohols **1**–**5** and their methylated ethers **7**–**11**. The ion fragments corresponding to $^{16}O$-$[M]^+$ and $^{18}O$-$[M]^+$ were monitored to analyze alcohols **6**, while the extent of labeling of its methylated ethers **12** was measured by using the corresponding $^{16}O$-$[M - CF_3]^+$ and $^{18}O$-$[M - CF_3]^+$ fragments.

**Computational details**: Quantum-chemical ab initio calculations were performed by using the Unix version of the Gaussian 98 set of programs[7] installed on an Alphaserver Compaq DS20E machine. The geometries of the investigated species were optimized, by analytical gradient techniques, at the HF/6–31G* level of theory. The located critical points were unambiguously characterized as true minima on the potential energy surface by computing, at the same computational level, the corresponding analytical vibrational frequencies. The latter values were used to calculate the zero-point vibrational energies (ZPE).

## Results

The main products from the γ-radiolysis of the gaseous $CH_3Cl/\mathbf{1_S}-\mathbf{6_R}$ systems are the corresponding retained and inverted methyl ethers, as well as the racemate of the starting alcohol (relative yields denoted in Table 1 as $Y_{retained}$, $Y_{inverted}$, and $Y_{racemate}$, respectively). These products are accompanied by appreciable amounts of the corresponding styrenes (relative yield denoted in Table 1 as $Y_{styrene}$).[8] Neither 2,3,4,5,6-pentafluorostyrene (**18**) is formed from alcohol $\mathbf{5_R}$, nor is racemization of alcohol $\mathbf{6_R}$ observed. The values in Table 1 represent the mean yield factors of the products, as obtained from several separate irradiations carried out under the same experimental conditions and whose reproducibility is expressed by the uncertainty level quoted. The ionic origins of the products are demonstrated by the sharp decrease (over 80%) of their abundance as the $(C_2H_5)_3N$ concentration is raised from approximately 0.1 to approximately 0.5 mol%.

While the $^{18}O$ content in racemate *rac*-**1**–*rac*-**5** amounts to approximately 40%, no detectable incorporation of the $^{18}O$ label is observed in the ethereal products **7**–**12** of Table 1. This observation excludes the involvement of water[9] at any stage of the formation of the ethereal products and points to the radiolytic $(CH_3)_2Cl^+$ ions as their exclusive precursors. The predominance of the retained ether over the inverted one under all conditions indicates that the attack of $(CH_3)_2Cl^+$ at the O center of the starting alcohols $\mathbf{1_S}-\mathbf{6_R}$ primarily yields the corresponding oxonium intermediates with the same configuration as the starting substrates, that is $\mathbf{I_S}-\mathbf{VI_R}$, respectively. Alkenes **14**–**17** and the partially labeled racemate of the starting alcohol[10] arise from the partial dissociation[11] of $\mathbf{I_S}-\mathbf{V_R}$ into the corresponding benzyl cations and $CH_3OH$ prior to its neutralization by the strong base B = $(C_2H_5)_3N$. No signs of the unimolecular dissociation of $\mathbf{VI_R}$ were observed.

Accordingly, formation of the products of Table 1 conforms to the reaction networks of Scheme 2. Their kinetic treatment leads to Equations (1)–(3).[12]

$$Y_{retained} = 0.5[e^{-k_{diss}\tau} + e^{-(2k_{inv}+k_{diss})\tau}] \quad (1)$$

$$Y_{inverted} = 0.5[e^{-k_{diss}\tau} - e^{-(2k_{inv}+k_{diss})\tau}] \quad (2)$$

$$Y_{styrene} + Y_{racemate} = 1 - e^{-k_{diss}\tau} \quad (3)$$

Table 1. Kinetics of gas-phase methylation-induced inversion and dissociation of chiral 1-arylethanols in the presence of $(C_2H_5)_3N$.

| System Composition [Torr][a] Substr. | $(C_2H_5)_3N$ | Reaction temp. [°C] | Reaction time ($\tau$) [$\times 10^8$ s][b] | Yield factor, **Y(M)**[c] $Y_{inverted}$ | $Y_{retained}$ | $Y_{racemate}$ | $Y_{styrene}$ | Rate constants ($\times 10^{-6}$ s$^{-1}$) $k_{inv}$[d] | $\log k_{inv}$ | $k_{diss}$[d] | $\log_{diss}$ |
|---|---|---|---|---|---|---|---|---|---|---|---|
| **$1_S$** | | | | **Y($7_R$)** | **Y($7_S$)** | **Y(*rac*-1)** | **Y(14)** | | | | |
| 0.61 | 1.23 | 60 | 2.3 | 0.034 | 0.966 | – | | 1.53 | 6.18 | – | |
| 0.51 | 1.19 | 70 | 2.5 | 0.058 | 0.942 | – | | 2.47 | 6.39 | – | |
| 0.63 | 1.19 | 80 | 2.6 | 0.110 | 0.890 | – | | 4.78 | 6.68 | – | |
| 0.51 | 1.18 | 100 | 2.7 | 0.137 | 0.863 | – | | 5.93 | 6.77 | – | |
| 0.63 | 1.22 | 120 | 2.8 | 0.226 | 0.774 | – | | 10.74 | 7.03 | – | |
| 0.60 | 1.18 | 140 | 3.0 | 0.313 | 0.687 | – | | 16.39 | 7.21 | – | |
| 0.61 | 1.20 | 160 | 3.2 | 0.414 | 0.586 | – | | 27.54 | 7.44 | – | |
| **$2_S$** | | | | **Y($8_R$)** | **Y($8_S$)** | **Y(*rac*-2)** | **Y(15)** | | | | |
| 0.33 | 0.80 | 60 | 3.7 | 0.079 | 0.634 | 0.103 | 0.184 | 3.39 | 6.53 | 9.14 | 6.96 |
| 0.22 | 0.56 | 70 | 5.4 | 0.100 | 0.466 | 0.249 | 0.185 | 4.05 | 6.61 | 10.55 | 7.02 |
| 0.40 | 0.80 | 80 | 3.9 | 0.076 | 0.497 | 0.146 | 0.281 | 3.93 | 6.59 | 14.29 | 7.16 |
| 0.44 | 0.81 | 80 | 3.9 | 0.087 | 0.486 | 0.165 | 0.262 | 4.61 | 6.66 | 14.28 | 7.15 |
| 0.40 | 0.79 | 100 | 4.2 | 0.091 | 0.362 | 0.118 | 0.429 | 6.08 | 6.78 | 18.87 | 7.28 |
| 0.40 | 0.80 | 120 | 4.4 | 0.082 | 0.191 | 0.033 | 0.694 | 10.47 | 7.02 | 29.56 | 7.47 |
| 0.43 | 0.83 | 140 | 4.4 | 0.037 | 0.074 | 0.068 | 0.821 | 12.30 | 7.09 | 49.94 | 7.70 |
| 0.50 | 0.81 | 160 | 4.8 | 0.020 | 0.031 | 0.094 | 0.855 | 16.46 | 7.22 | 61.83 | 7.79 |
| **$3_S$** | | | | **Y($9_R$)** | **Y($9_S$)** | **Y(*rac*-3)** | **Y(16)** | | | | |
| 0.27 | 0.35 | 40 | 8.1 | 0.029 | 0.924 | 0.046 | nd | 0.40 | 5.60 | 0.57 | 5.76 |
| 0.26 | 0.46 | 60 | 6.6 | 0.052 | 0.866 | 0.077 | 0.005 | 0.90 | 5.96 | 1.26 | 6.10 |
| 0.24 | 0.46 | 80 | 7.0 | 0.104 | 0.571 | 0.277 | 0.048 | 2.61 | 6.42 | 5.63 | 6.75 |
| 0.25 | 0.71 | 120 | 5.1 | 0.097 | 0.152 | 0.207 | 0.544 | 14.83 | 7.17 | 27.24 | 7.43 |
| 0.24 | 0.63 | 140 | 6.0 | 0.037 | 0.040 | 0.137 | 0.786 | 27.82 | 7.44 | 42.81 | 7.66 |
| **$4_S$** | | | | **Y($10_R$)** | **Y($10_S$)** | **Y(*rac*-4)** | **Y(17)** | | | | |
| 0.20 | 0.68 | 25 | 4.0 | 0.025 | 0.975 | nd | nd | 0.64 | 5.81 | nd | nd |
| 0.21 | 0.89 | 40 | 3.2 | 0.032 | 0.913 | 0.055 | nd | 1.10 | 6.04 | 1.78 | 6.25 |
| 0.26 | 0.69 | 60 | 4.4 | 0.078 | 0.761 | 0.095 | 0.066 | 2.34 | 6.37 | 3.98 | 6.60 |
| 0.32 | 0.63 | 80 | 5.1 | 0.136 | 0.516 | 0.212 | 0.136 | 5.31 | 6.72 | 8.44 | 6.93 |
| 0.39 | 0.60 | 100 | 5.7 | 0.112 | 0.226 | 0.190 | 0.472 | 9.51 | 6.98 | 19.01 | 7.28 |
| 0.22 | 0.66 | 120 | 5.5 | 0.102 | 0.148 | 0.052 | 0.698 | 15.39 | 7.19 | 25.22 | 7.40 |
| **$5_R$** | | | | **Y($11_S$)** | **Y($11_R$)** | **Y(*rac*-5)** | **Y(18)** | | | | |
| 0.62 | 0.46 | 25 | 5.2 | 0.004 | 0.979 | 0.017 | nd | 0.08 | 4.89 | 3.22 | 5.51 |
| 0.70 | 0.49 | 60 | 6.2 | 0.024 | 0.878 | 0.098 | nd | 0.43 | 5.63 | 1.58 | 6.20 |
| 0.71 | 0.51 | 85 | 6.5 | 0.031 | 0.423 | 0.546 | nd | 1.14 | 6.06 | 12.16 | 7.08 |
| 0.80 | 0.54 | 120 | 6.8 | 0.078 | 0.265 | 0.657 | nd | 4.48 | 6.65 | 15.74 | 7.20 |
| 0.99 | 0.42 | 160 | 9.6 | 0.001 | 0.001 | 0.998 | nd | 12.30 | 7.09 | 79.43 | 7.90 |
| **$6_R$** | | | | **Y($12_S$)** | **Y($12_R$)** | **Y(*rac*-6)** | | | | | |
| 0.37 | 0.29 | 85 | 9.2 | 0.015 | 0.985 | nd | | 0.16 | 5.22 | $< 0.01$ | |
| 0.37 | 0.27 | 100 | 12.4 | 0.027 | 0.973 | nd | | 0.22 | 5.35 | $< 0.01$ | |
| 0.38 | 0.25 | 120 | 14.2 | 0.099 | 0.901 | nd | | 0.78 | 5.89 | $< 0.01$ | |
| 0.38 | 0.30 | 140 | 12.5 | 0.220 | 0.780 | nd | | 2.32 | 6.36 | $< 0.01$ | |
| 0.38 | 0.26 | 160 | 15.2 | 0.290 | 0.710 | nd | | 2.85 | 6.46 | $< 0.01$ | |

[a] $CH_3Cl$: 720 Torr, $H_2{}^{18}O$: 2–3 Torr; $O_2$: 4 Torr. Radiation dose: $2x10^4$ Gy (dose rate: $1x10^4$ Gy h$^{-1}$). [b] Reaction time, $\tau$, calculated from the reciprocal of the first-order collision constant between the relevant methyloxonium intermediate and $(C_2H_5)_3N$ (see text). [c] The relative yield of *rac*-**1**/*rac*-**5** is calculated by doubling the yield of the inverted starting alcohol (ref. [8]). Each value is the average of several determinations, with an uncertainty level of about 5%. nd: **Y(M)** $< 0.001$. The dashes denote that formation of **14** by far predominates under all conditions. [d] See text.

The $k_{inv}$ and $k_{diss}$ rate constants, derived from Equations (1)–(3), are expressed as Equations (4) and (5), respectively.

$$k_{inv} = 0.5\tau^{-1}\{\ln[(Y_{retained} + Y_{inverted})/(Y_{retained} - Y_{inverted})]\} \quad (4)$$

$$k_{diss} = \tau^{-1}\{\ln[1 - (Y_{styrene} + Y_{racemate})]^{-1}\} \quad (5)$$

The $\tau$ term represents the lifetime of intermediates **I–VI** before deprotonation by the base B ($(C_2H_5)_3N$). When the efficiency of the ion deprotonation by B (e.g. $k_b$ in Scheme 2) is set to one, $\tau$ is expressed by $(k_b[B])^{-1}$.[13] The Arrhenius plots of $k_{inv}$ and $k_{diss}$ for $\mathbf{II_S}$ over the 60–160 °C temperature range are reported in Figure 1. Similar plots are obtained for $\mathbf{III_S}$, $\mathbf{IV_S}$, and $\mathbf{V_R}$. In the case of $\mathbf{I_S}$, dissociation largely predominates over inversion, suggesting that the inversion barrier is very close to the dissociation limit. No dissociation is observed for $\mathbf{VI_R}$ within the temperature range investigated (85–160 °C), indicating that its dissociation free energy exceeds 15 kcalories per mol at 100 °C.

Figure 2 and Figure 3, respectively, report the Arrhenius plots of $k_{inv}$ and $k_{diss}$ for all the selected alcohols, together with that concerning the O-methylation of (*R*)-(+)-1-phenylethanol ($\mathbf{VII_R}$) already described in a previous paper.[4] The

  

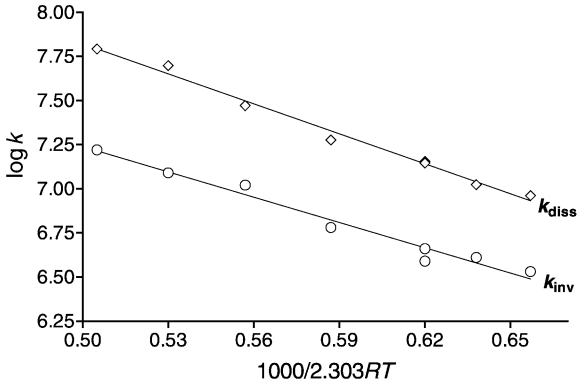


Figure 1. Arrhenius plots for the $\mathbf{II_S}\longrightarrow\mathbf{II_R}$ intracomplex inversion ($k_{inv}$) and the $\mathbf{II_S}\longrightarrow$*para*-$ClC_6H_4CHCH_3^+ + CH_3OH$ dissociation ($k_{diss}$).

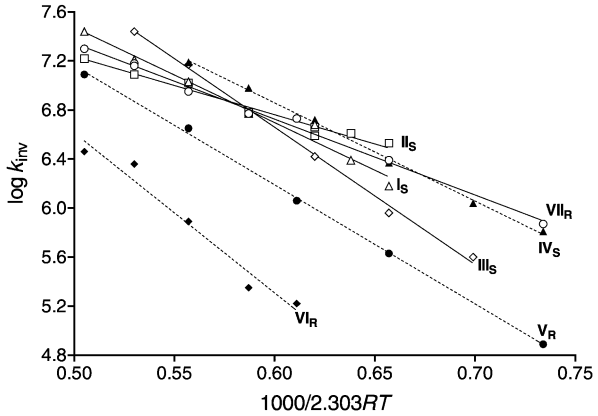


Figure 2. Arrhenius plots for the inversion of configuration of the selected oxonium intermediates.

relevant linear curves obey the equations reported in Table 2 and Table 3, respectively. The tables give the relevant activation parameters, as calculated from the transition-state theory.

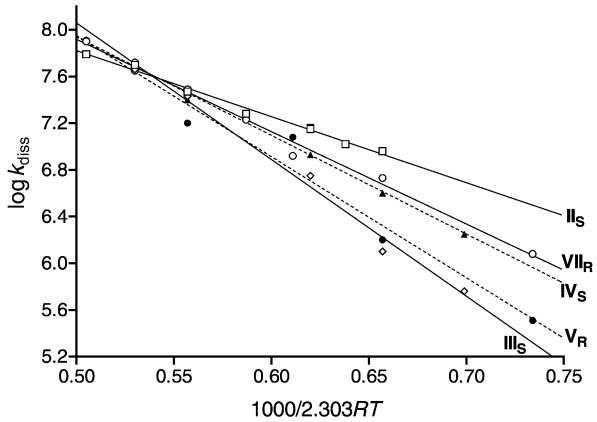


Figure 3. Arrhenius plots for the dissociation of the selected oxonium intermediates.

## Discussion

**Isokinetic relationships**: The solid lines of Figure 2, concerning the inversion of configuration of $\mathbf{I_S}$, $\mathbf{II_S}$, $\mathbf{III_S}$, and $\mathbf{VII_R}$ (henceforth denoted as the F family), exhibit a distinct point of common intersection at a temperature falling within the range investigated (25–160 °C). A similar common intersection region, concerning the inversion of configuration of $\mathbf{IV_S}$, $\mathbf{V_R}$, and $\mathbf{VI_R}$ (henceforth denoted as the G family, broken lines in Figure 2) and not graphically illustrated in the figure, is located above the temperature range investigated. The curves of Figure 3, concerning the dissociation of $\mathbf{II_S}$, $\mathbf{III_S}$, $\mathbf{IV_S}$, $\mathbf{V_R}$, and $\mathbf{VII_R}$ (henceforth denoted as the E family), also display a point of common intersection at a temperature close to the upper extreme of the temperature range investigated.

These common intersections can safely be regarded as originating from genuine isokinetic relationships (IKR).[14] This is demonstrated by the excellent linearity of the corresponding $\Delta H^*_{inv}$ versus $\Delta S^*_{inv}$ plots for the F family inversion (corr. coeff.: $r^2 = 0.9999$; standard deviation:

Table 2. Arrhenius parameters for the gas-phase intracomplex inversion of O-protonated 1-aryl-1-methoxyethanes.

| Process | Arrhenius equation ($y = 1000/2.303\,RT$) | Corr. coeff. ($r^2$) | $\Delta H^*_{inv}$ [kcal mol$^{-1}$] | $\Delta S^*_{inv}$ [cal mol$^{-1}$ K$^{-1}$] |
|---|---|---|---|---|
| $\mathbf{I_S}\longrightarrow\mathbf{I_R}$ | $\log k_{inv} = (11.3\pm0.3) - (7.8\pm0.5)y$ | 0.978 | $7.0\pm0.5$ | $-9.0\pm0.9$ |
| $\mathbf{II_S}\longrightarrow\mathbf{II_R}$ | $\log k_{inv} = (9.6\pm0.2) - (4.8\pm0.3)y$ | 0.973 | $4.0\pm0.4$ | $-16.9\pm0.9$ |
| $\mathbf{III_S}\longrightarrow\mathbf{III_R}$ | $\log k_{inv} = (13.3\pm0.2) - (11.1\pm0.3)y$ | 0.997 | $10.4\pm0.3$ | $+0.1\pm1.1$ |
| $\mathbf{VII_R}\longrightarrow\mathbf{VII_S}$ | $\log k_{inv} = (10.4\pm0.1) - (6.2\pm0.2)y$ | 0.994 | $5.4\pm0.3$ | $-13.3\pm1.0$ |
| $\mathbf{IV_S}\longrightarrow\mathbf{IV_R}$ | $\log k_{inv} = (11.7\pm0.1) - (8.0\pm0.2)y$ | 0.998 | $7.3\pm0.3$ | $-7.4\pm0.8$ |
| $\mathbf{V_R}\longrightarrow\mathbf{V_S}$ | $\log k_{inv} = (12.0\pm0.1) - (9.7\pm0.2)y$ | 0.999 | $8.9\pm0.2$ | $-5.4\pm0.5$ |
| $\mathbf{VI_R}\longrightarrow\mathbf{VI_S}$ | $\log k_{inv} = (13.1\pm0.8) - (13.0\pm1.5)y$ | 0.964 | $12.3\pm1.5$ | $-0.9\pm1.0$ |

Table 3. Arrhenius parameters for the gas-phase dissociation of O-protonated 1-aryl-1-methoxyethanes.

| Process | Arrhenius equation ($y = 1000/2.303\,RT$) | Corr. coeff. ($r^2$) | $\Delta H^*_{inv}$ [kcal mol$^{-1}$] | $\Delta S^*_{inv}$ [cal mol$^{-1}$ K$^{-1}$] |
|---|---|---|---|---|
| $\mathbf{II_S}\longrightarrow p ClC_6H_4CHCH_3^+ + MeOH$ | $\log k_{diss} = (10.6\pm0.1) - (5.7\pm0.2)y$ | 0.989 | $4.9\pm0.3$ | $-12.2\pm0.7$ |
| $\mathbf{III_S}\longrightarrow m CF_3C_6H_4CHCH_3^+ + MeOH$ | $\log k_{diss} = (13.9\pm0.4) - (11.7\pm0.7)y$ | 0.990 | $10.9\pm0.6$ | $+2.6\pm2.0$ |
| $\mathbf{VII_R}\longrightarrow C_6H_5CHCH_3^+ + MeOH$ | $\log k_{diss} = (11.9\pm0.3) - (7.9\pm0.2)y$ | 0.992 | $7.1\pm0.3$ | $-6.7\pm1.2$ |
| $\mathbf{IV_S}\longrightarrow p CF_3C_6H_4CHCH_3^+ + MeOH$ | $\log k_{diss} = (12.1\pm0.3) - (8.4\pm0.5)y$ | 0.990 | $7.7\pm0.5$ | $-5.4\pm1.4$ |
| $\mathbf{V_R}\longrightarrow C_6F_5CHCH_3^+ + MeOH$ | $\log k_{diss} = (13.1\pm0.7) - (10.3\pm1.1)y$ | 0.965 | $9.6\pm1.1$ | $-0.9\pm1.9$ |

$sd = 0.028$) (solid line in Figure 4), for the G family inversion (corr. coeff.: $r^2 = 0.9998$, standard deviation: $sd = 0.049$) (broken line in Figure 4), and for the E family dissociation (corr. coeff.: $r^2 = 0.9995$, standard deviation: $sd = 0.063$) (Figure 5), whose statistical uncertainties are well within the experimental errors.

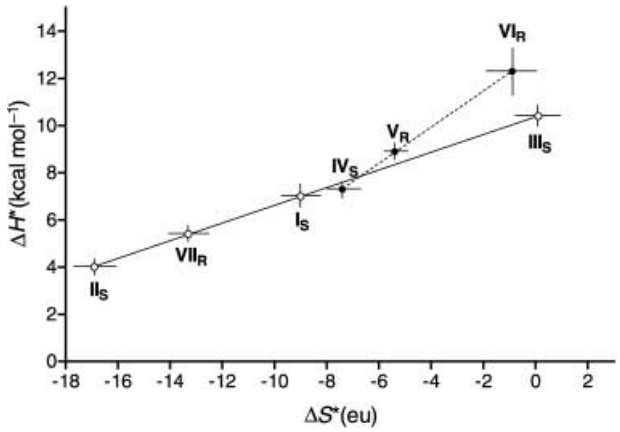


Figure 4. Enthalpy – entropy compensation plots for the inversion of $\mathbf{I_S}$, $\mathbf{II_S}$, $\mathbf{III_S}$, and $\mathbf{VII_R}$ (the F family) and $\mathbf{IV_S}$, $\mathbf{V_R}$, and $\mathbf{VI_R}$ (the G family).

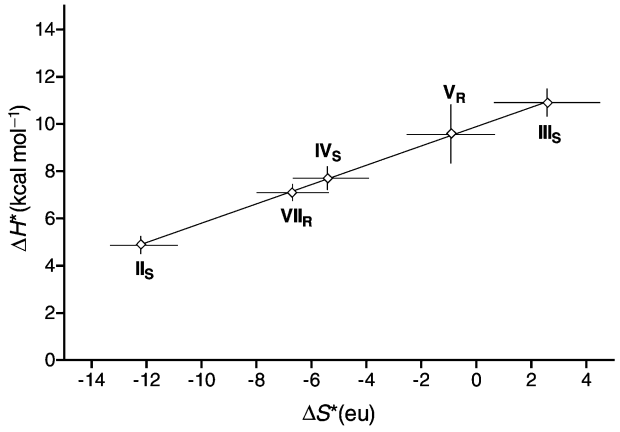


Figure 5. Enthalpy – entropy compensation plot for the dissociation of $\mathbf{II_S}$, $\mathbf{III_S}$, $\mathbf{IV_S}$, $\mathbf{V_R}$, and $\mathbf{VII_R}$ (the E family).

Indeed, the maximum errors in $\Delta H^*_{inv}(\delta)$ and $\Delta S^*_{inv}(\sigma)$ are 1.5 kcal mol$^{-1}$ and 1.1 cal K$^{-1}$ mol$^{-1}$ (Table 2), and $\delta =$ 1.1 kcal mol$^{-1}$ and $\sigma = 2.0$ cal K$^{-1}$ mol$^{-1}$ (Table 3). The error criterion is satisfied in the present study, that is $\Delta H^*_{inv} > 2\delta$ and $\Delta\Delta S^*_{inv} > 2\sigma$, and hence the $\Delta H^*_{inv}$ versus $\Delta S^*_{inv}$ correlations of Figure 4 and Figure 5 are real.

The curves of Figure 4 show the existence of two different enthalpy – entropy compensation effects on the *gas-phase inversion* of the **I – VII** ions, related to the nature and the position of the substituent(s) in their structure. In contrast, the curve of Figure 5 points to the existence of a single enthalpy – entropy compensation in the *gas-phase dissociation* of the same ions.

The definition of an IKR implies that, at the isokinetic temperature ($T_{iso}$), $\Delta G^*_{iso} = \Delta H^* - T_{iso}\Delta S^* = \text{const}$. Therefore, the slopes of the linear curves of Figure 4 and Figure 5 provide the relevant $T_{iso}$ values, while the Y intercepts give an estimate of the corresponding $\Delta G^*_{iso}$ terms. Accordingly, the isokinetic parameters for the F inversion reactions are $T_{iso} = 376 \pm 2$ K, $\Delta G^*_{iso} = 10.37 \pm 0.02$ kcal mol$^{-1}$, and $\log k_{iso} = 6.84$, whereas those for the G inversion reactions are $T_{iso} = 767 \pm 10$ K, $\Delta G^*_{iso} = 13.00 \pm 0.05$ kcal mol$^{-1}$, and $\log k_{iso} = 9.35$. Similarly, the isokinetic parameters for the E dissociations are $T_{iso} = 409 \pm 5$ K, $\Delta G^*_{iso} = 9.89 \pm 0.04$ kcal mol$^{-1}$, and $\log k_{iso} = 7.61$.

**Activation dynamics**: Several theories have been advanced to provide insight into the origin of IKRs. Linert's model[15] is based on Kramer's view[16] of reactant molecules (M), activated by quantum-mechanical energy exchange with molecules of the surrounding medium acting as a constant-temperature "heat bath" (HB). After a random walk over discrete energy levels of the reactants, they reach, at the highest point of the barrier, a point of no return. The crossing of this barrier constitutes the chemical reaction rate.

At the thermal equilibrium, an equation is obtained for the rate constant, which depends on the collision number, the energy-barrier height, the temperature of the "heat bath", and the quantum-mechanical transition probability between any reactant level and the point of no return. When the "heat bath" contains energy stored in the form of vibrational degrees, the transition probabilities for vibrational – vibrational energy transfer are expressed by $P_{l,m} = l\exp(\omega/\nu)$(where $m$ is the HB vibrational level associated with $\nu$ and $l$ is that associated with M) and reach the maximum value for a *resonant* vibrational – vibrational coupling when $\nu m = \omega l$.

In the condensed phase, cooperative supramolecular effects normally make HB vibrational frequencies ($\nu$) available that are much smaller than those of M ($\omega$). In this case, the only variable parameter for a family of reactions is $\omega$ and, therefore, the IKR can be expressed mathematically as $d\ln k(\omega)/d\omega = 0$ at $T_{iso}$.

Accordingly, for a homogeneous family of reactions such as that of the present investigation, a single $T_{iso}$ should be found whose value (in K) corresponds to the characteristic vibrational frequency $\nu$ (in cm$^{-1}$) predominantly exchanging energy in the HB ([Eq. (6)]; $k_B$ = Botzmann constant; $h$ = Planck constant).

$$T_{iso} = \frac{h\nu}{2k_B} = 0.719\nu \qquad (6)$$

While this is the case for the gas-phase E dissociation (Figure 3 and Figure 5), the observation in the same gaseous HB ($CH_3Cl$ at 720 Torr) of *two isokinetic temperatures* for the **I – VII** inversion (Figure 2 and Figure 4) underlines the existence of a point of discontinuity in the $\nu/\omega$ coupling. This may be peculiar for gaseous media where cooperative supramolecular effects are negligible and thus $\nu$ and $\omega$ are both variable parameters for a family of reactions.[15]

In this frame, the two isokinetic relationships of Figure 4 can be rationalized in terms of Larsson's selective energy transfer (SET) model,[17] which introduces in Linert's model the notion of several possible switchovers in the resonant $\nu/\omega$ coupling. Thus, in the assumption of full $\nu/\omega$ resonance ([Eq. (6)], $T_{iso} = 376 \pm 2$ K for the inversion of configuration of the F family corresponds to a vibrational frequency $\nu_F$ predom-

  

inantly exchanging energy of $523 \pm 3\ cm^{-1}$, whereas $T_{iso} = 767 \pm 10$ K the inversion of the G family corresponds to a predominant vibrational frequency $\nu_G = 1067 \pm 14\ cm^{-1}$. According to theory, these frequencies should correspond to intense absorption bands of the vibrational spectrum of gaseous $CH_3Cl$.

As a matter of fact, the IR spectrum of gaseous $CH_3Cl$ shows characteristic vibrational bands around 1015 $cm^{-1}$ and 732 $cm^{-1}$, which are assigned to its $\nu_6(e)$ $CH_3$-rocking and $\nu_3(a_1)$ C–Cl stretching modes, respectively.[18–20] The same spectrum does not show any significant band below $\nu_3(a_1)$. The $\nu_G = 1067 \pm 14\ cm^{-1}$ value, corresponding to $T_{iso} = 767 \pm 10$ K for the G family under the full resonance assumption, closely approaches $\nu_6(e)$ (Figure 6).

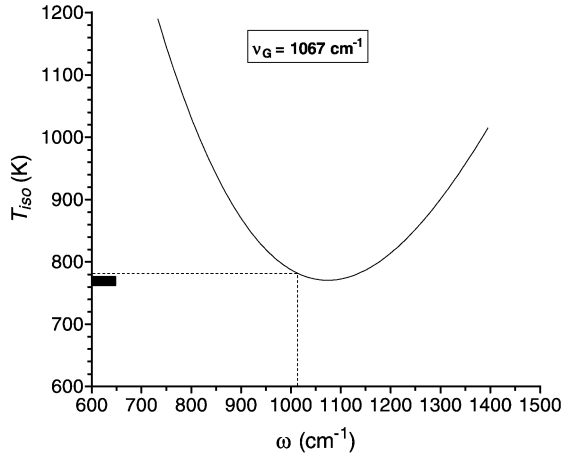


Figure 6. Dependence of the isokinetic temperature ($T_{iso}$) as a function of the critical vibrational frequency of the G reactant (ω, [Eq. (7)]), taking the resonant $\nu_G = 1067\ cm^{-1}$ value calculated from Equation (1) as the critical frequency of $CH_3Cl$. The broken line on the *x* axis refers to the actual $\nu_6(e) = 1015\ cm^{-1}$ $CH_3$ rocking mode of the unperturbed $CH_3Cl$ molecule [refs. 18–20]. The black bar on the y axis shows the $T_{iso} = 767 \pm 10$ K measured from the isokinetic relationship for the inversion of configuration of G (Figure 4).

This means that the unimolecular rearrangement of G is essentially promoted by *resonant* energy exchange with the $CH_3$-rocking mode of $CH_3Cl$. On the contrary, none of the characteristic absorption bands of the $CH_3Cl$ spectrum can account for the value of $T_{iso} = 376 \pm 2$ K obtained for the F series. Indeed, even considering the possibility of *nonresonant* energy exchange with the lowest available $CH_3Cl$ frequency ($\nu_3(a_1) = 732\ cm^{-1}$), the minimum $T_{iso}$ value, calculated from Equation (7) as a function of ω for the F series,[17] always exceeds the actual value (376 ± 2 K) by no less than 123 K (Figure 7).

$$T_{iso} = \frac{\dfrac{h[\nu^2 - \omega^2]}{k_B \omega}}{\left[\pm^{\pi}/_2 - \text{arctg}\dfrac{\nu\omega}{2(\nu^2 - \omega^2)}\right]} \qquad (7)$$

This implies the operation of two different activation dynamics for the inversion of configuration of the oxonium ions **I–VII**. The activation dynamics of the G ions involves the *resonant* energy exchange between their characteristic

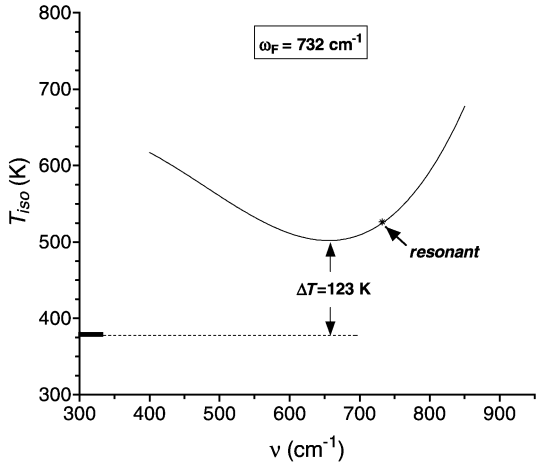


Figure 7. Dependence of the isokinetic temperature ($T_{iso}$) as a function of the critical vibrational frequency of $CH_3Cl$ (ν, [Eq. (7)], taking the critical frequency of the inversion of the F reactant ($\omega_F$) equal to that of the C–Cl stretching mode of the unperturbed $CH_3Cl$, that is $\nu_3(a_1) = 732\ cm^{-1}$. The asterisk denotes the resonant coupling between $\nu_3(a_1)$ and $\omega_F$. The black bar on the y axis shows the $T_{iso} = 376 \pm 2$ K measured from the isokinetic relationship for the inversion of configuration of F (Figure 4).

vibration frequency $\omega_G$ and the $CH_3$-rocking mode of $CH_3Cl$ ($\nu_6(e)$) (Figure 6). The lack of any correspondence between the estimated characteristic vibration frequency of the F ions ($\omega_F = 523 \pm 3\ cm^{-1}$) and any of the fundamental vibrational modes of the $CH_3Cl$ molecule (Figure 7), points to the activation of the F ions as proceeding by a more intimate mechanism involving their transient complexation with a $CH_3Cl$ molecule. Indeed, detailed theoretical and spectroscopic analyses of van der Waals complexes between $CH_3Cl$ and strong acids AH, both in the gas phase and in liquefied inert gases, point to the development of low-frequency Cl···H–A libration and torsional modes in their van der Waals complexes, falling in the mid-infrared region (500–300 $cm^{-1}$).[21,25]

Accordingly, HF/6–31G* calculations of a model complex between O-protonated benzyl methyl ether[26] and $CH_3Cl$ indicate the presence of nine vibrational frequencies additional to those characteristic of the two isolated components. Among these that for the out-of-plane C–Cl···H–O bending mode occurs at 639 $cm^{-1}$. Scaling down this value by 0.8953,[27] leads to a frequency value of 572 $cm^{-1}$ which may be compatible with $\omega_F = 523 \pm 3\ cm^{-1}$.

The same vibrational mode at 572 $cm^{-1}$ coincides with the critical value of $\omega_{diss} = 569\ cm^{-1}$ calculated from Equation (1) for the dissociation of the E family ($T_{iso} = 409 \pm 5$ K).

**Transition states and reaction dynamics**: The reaction dynamics of the oxonium ions **I–VII** are strictly related to their activation dynamics. The points of no return for the F inversion of configuration (henceforth denoted as $TS_F$) and of the E family dissociation, are attained by the out-of-plane C–Cl···H–O bending vibration in the intimate encounter complexes of the oxonium ions with $CH_3Cl$.

Some insights into the nature of $TS_F$ can be obtained from the inspection of Figure 8, showing the *energetically most favored* B3-LYP/6–31G*-calculated TS **VIII**, involved in the

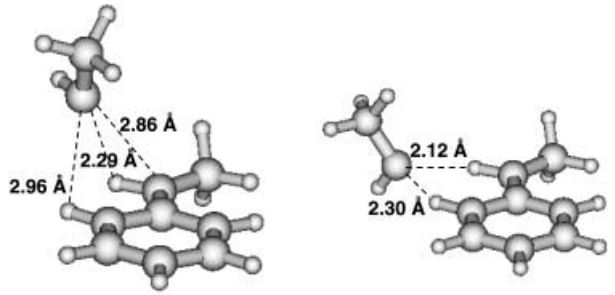


Figure 8. B3-LYP/6 – 31G*-optimized geometries of the critical structures on the $[C_6H_5CH^+CH_3,CH_3OH]$ potential energy hypersurface.

**VII$_R$**⟶**VII$_S$** inversion reaction.[4] Structure **VIII** exhibits a pronounced $C_\alpha$–O bond distance between the leaving $CH_3OH$ molecule and the planar α-methylbenzyl cation (2.86 Å). The $CH_3OH$ moiety establishes electrostatic interactions with the acidic α ($H_\alpha$) and *ortho* ($H_{ortho}$) hydrogen atoms of the benzyl ion in much the same way as in the inversion intermediate **IX**. It is concluded that the specific mode of activation of the F members of the family allows access to the *energetically most-favored* $TS_F$, characterized by the $C_\alpha$–O bond bending coupled with its elongation assisted by the rest of the complex. The similarity in the activation dynamics of the F inversion and the E dissociation suggests that both processes follow similar reaction coordinates.

The coordination of the $CH_3OH$ moiety with $H_\alpha$ and $H_{ortho}$ of the benzylic residue, and the intimate association of a $CH_3Cl$ molecule in the TS, may provide an explanation for lack of any correlation between the inversion rate constants of F (Table 1) and any simple combination of field/inductive and resonance effects of their substituents.[28] Indeed, according to $TS_F$, the ring substituent in the benzylic moiety exerts its effects not only toward the $C_\alpha$ reaction site, but also on the acidity and, hence, the coordinating properties of $H_{ortho}$.

The two isokinetic relationships of Figure 4 imply that the G inversion reaction proceeds through a reaction coordinate and a transition state (henceforth denoted as $TS_G$) which are substantially different from those involved in the F inversion reaction. The activation dynamics of the G inversion does not necessarily require intimate complexation with $CH_3Cl$. Indeed, the point of no return of the G inversion reaction is achieved by resonant coupling with the $\nu_6(e) = 1015\ cm^{-1}$ $CH_3$-rocking mode of an unperturbed $CH_3Cl$ molecule. A plausible model for $TS_G$ could involve the $C_\alpha$–O bond breaking *without any significant coordination* of the migrating $CH_3OH$ moiety with the acidic hydrogen atoms of the benzylic residue. This view is supported by the less negative $\Delta S^*_{inv}$ values measured for the inversion of the G members of the series relative to those of the F ions (except **III$_S$**)[29] (Table 2).

## Conclusion

Two different isokinetic relationships are observed in the gas-phase configuration inversion of a family of O-protonated 1-aryl-1-methoxyethanes, depending upon the nature and the position of the substituents. Since these were observed in exactly the same gaseous medium ($CH_3Cl$), the dual behavior is rationalized in terms of two different inversion dynamics driven by the activation dynamics from the bulk gas. Thus, if activation proceeds predominantly through a resonant energy exchange with the $\nu_6(e) = 1015\ cm^{-1}$ $CH_3$-rocking mode of the unperturbed molecule of the bath gas ($CH_3Cl$), the inversion reaction proceeds through the *dynamically most accessible* TS, involving unassisted $C_\alpha$–O bond rupture (the G family). If, instead, activation involves the out-of-plane C–Cl···H–O bending vibration developed in the intimate encounter complex between $CH_3Cl$ and the oxonium ions, the inversion reaction proceeds through the *energetically most accessible* TS. Here the $CH_3OH$ motion is assisted by coordination with the acidic hydrogen atoms of the benzylic residue (the F family). The same vibrational mode is active in promoting the dissociation of most members (**I – VII**) of the family of oxonium ions, irrespective of their belonging to the F or G sets. Since the G inversion reaction does not require any significant coordination with the $CH_3Cl$ molecules, its mechanism can be considered as essentially "unimolecular". In contrast, both the F inversion and the E dissociation can be regarded as "bimolecular" processes, since they involve intimate coordination with a $CH_3Cl$ molecule. Their transition states, characterized by extensive coordination of the $CH_3OH$ moiety with the $H_\alpha$ and $H_{ortho}$ atoms of the benzylic residue, justify the observation that, despite the relevant activation parameters conforming to isokinetic relationships, they nevertheless do not obey any linear free-energy relationships.[30]

The results of the present study show, for the first time, the possible coexistence of different activation dynamics in the gas phase and their strict connection with the dynamics and the mechanism of ionic reactions. Competing processes, namely the F inversion and the E dissociation, are promoted by the same activation dynamics. Instead, the same ionic reaction, namely the **I – VII** inversion of configuration, can be promoted by different activation dynamics depending upon the nature and the position of the substituents.

## Acknowledgement

This work was supported by the Ministero della Istruzione, dell'Università, e della Ricerca Scientifica (MIUR) and the Consiglio Nazionale delle Ricerche (CNR). We thank F. Gasparrini for his assistance in the isolation of the pure enantiomers of the starting chiral alcohols. Thanks are also due to F. Grandinetti for his support in the theoretical calculations and to F. Cacace for helpful discussions.

[1] See, for instance: J. P. Richard, Y. Tsuji, *J. Am. Chem. Soc.* **2000**, *122*, 3963, and references therein.
[2] a) M. V. Merritt, S. J. Bell, H. J. Cheon, J. A. Darlington, T. L. Dugger, N. B. Elliott, G. L. Fairbrother, C. S. Melendez, E. V. Smith, P. L. Schwartz, *J. Am. Chem. Soc.* **1990**, *112*, 3560, and references therein; b) M. V. Merritt, D. B. Anderson, K. A. Basu, I. W. Chang, H. J. Cheon, N. E. Mukundan, C. A. Flannery, A. Y. Kim, A. Vaishampayan, D. A. Yens, *J. Am. Chem. Soc.* **1994**, *116*, 5551, and references therein.
[3] A Thibblin, *J. Phys. Org. Chem.* **1993**, *6*, 287, and references therein.
[4] A. Filippi, F. Gasparrini, M. Speranza, *J. Am. Chem. Soc.* **2001**, *123*, 2251

  

[5] D. Achet, D. Rocrelle, I. Murengezi, A. Delmas, A. Gaset, *Synthesis* **1986**, 643.
[6] S. G. Lias, E. P. L. Hunter, *J. Phys. Chem. Ref. Data* **1998**, *27*, 413.
[7] M. J. Frish, G. W. Trucks, H. B. Schlegel, G. E. Scuseria, M. A. Robb, J. R. Cheeseman, V. G. Zakrzewski, J. A. Montgomery, Jr., R. E. Stratman, J. C. Burant, S. Dapprich, J. M. Millam, A. D. Daniels, K. N. Kudin, M. C. Strain, O. Farkas, J. Tomasi, V. Barone, M. Cossi, R. Cammi, B. Mennucci, C. Pomelli, C. Adamo, S. Clifford, J. Ochterski, G. A. Petersson, P. Y. Ayala, Q. Cui, K. Morokuma, D. K. Malik, A. D. Rabuck, K. Raghavachari, J. B. Foresman, J. Cioslowski, J. V. Ortiz, A. G. Raboul, B. B. Stefaniv, G. Liu, A. Liashenko, P. Piskorz, I. Nanayakkara, C. Gonzales, M. Challacombe, P. M. W. Gill, B. Johnson, W. Chen, M. W. Wong, J. L. Andres, C. Gonzales, M. Head-Gordon, E. S. Replogle, J. A. Pople, Gaussian 98, Revision *A7*, Gaussian, Inc., Pittsburg, PA, 1998.
[8] Owing to the presence of the starting alcohols $\mathbf{1_S}-\mathbf{5_R}$, the extent of their back association ($k_W$) of Scheme 2 cannot be directly determined. However, enantioselective HRGC-MS analysis reveals the formation of $^{18}$O-labeled inverted alcohol in concentrations equal to that of the retained $^{18}$O-labeled enantiomer. On these grounds, the overall abundance of the retained alcohol can be taken as equal to that of the inverted one and, therefore, the yield factor of *rac*-**1**–*rac*-**5** can be estimated by doubling that of inverted alcohol.
[9] The irradiated systems invariably contain $H_2{}^{16}O$, as ubiquitous impurity either initially introduced in the mixture together with its bulk component or formed from its radiolysis. As pointed out previously (A. Troiani, F. Gasparrini, F. Grandinetti, M. Speranza, *J. Am. Chem. Soc.* **1997**, *119*, 4525; M. Speranza, A. Troiani, *J. Org. Chem.* **1998**, *63*, 1020), the average stationary concentration of $H_2{}^{16}O$ in the radiolytic systems is estimated to approach that of the added $H_2{}^{18}O$ (approximately 2–3 Torr).
[10] The conceivable bimolecular $H_2{}^{18}O$-to-$CH_3OH$ displacement on $\mathbf{I_S}-\mathbf{V_R}$ as a route to racemate ***rac*-1**–***rac*-5** is ruled out on both stereochemical and thermochemical grounds. For instance, $H_2O$-to-$CH_3OH$ substitution on O-protonated benzyl methyl ether is 14.4 kcal mol$^{-1}$ endothermic.
[11] Kinetic predominance of proton transfers over β-eliminative processes allows us to assign the formation of styrenes to deprotonation of the corresponding benzyl cations by $(C_2H_5)_3N$.
[12] J. Andraos, *J. Chem. Educ.* **1999**, *76*, 1578.
[13] The collision constants $k_b$ of Scheme 2 are calculated according to: T. Su, W. J. Chesnavitch, *J. Chem. Phys.* **1982**, *76*, 5183.
[14] L. Liu, Q. X. Guo, *Chem. Rev.* **2001**, *101*, 673, and references therein.
[15] W. Linert, R. F. Jameson, *Chem. Soc. Rev.* **1989**, *18*, 477, and references therein.
[16] H. A. Kramer, *Physica* **1940**, *7*, 284.
[17] R. Larsson, *Catal. Today* **1988**, *3*, 387.
[18] E. F. Barker, E. K. Plyler, *J. Chem. Phys.* **1935**, *3*, 367.
[19] W. H. Bennett, C. F. Meyer, *Phys. Rev.* **1928**, *32*, 888.
[20] H. D. Noether, *J. Chem. Phys.* **1942**, *10*, 664.
[21] K. Uehara, T. Shimizu, K. Shimoda, *IEEE J. Quantum Electron.* **1968**, *4*, 728.
[22] D. M. Bishop, *J. Chem. Phys.* **1993**, *98*, 3179.
[23] W. A. Herrebout, B. J. van der Veken, J. R. Durig, *J. Molec. Struct. (TEOCHEM)* **1995**, *332*, 231.
[24] W. A. Herrebout, B J. van der Veken, *J. Phys. Chem.* **1993**, *97*, 10622.
[25] R. T. Arlinghaus, L. Andrews, *J. Phys. Chem.* **1984**, *88*, 4032.
[26] O-Protonated benzyl methyl ether was considered instead of $\mathbf{VII_R}$ to reduce the size of the calculation.
[27] A. P. Scott, L. Radom, *J. Phys. Chem.* **1996**, *100*, 16502.
[28] C. Hansch, A. Leo, R. W. Taft, *Chem. Rev.* **1991**, *91*, 55.
[29] A reason for the large $\Delta S^*_{inv}$ for the inversion of $\mathbf{III_S}$ can be found in the observation that group polarizability and field/inductive factors are more effective than resonance factors in the gas phase (ref. [28]). Accordingly, the *meta*-$CF_3$ group in $\mathbf{III_S}$ ($\Delta H^*_{inv} = 10.4 \pm 0.3$ kcal mol$^{-1}$) hinders inversion more than the *para*-$CF_3$ group in $\mathbf{IV_S}$ ($\Delta H^*_{inv} = 7.3 \pm 0.3$ kcal mol$^{-1}$), since it is closer to the $C_\alpha$ reaction center. As pointed out in the text, the activation energy is partially compensated for in $TS_F$ by multiple coordination of $CH_3OH$ with the $H_\alpha$ atom of the benzylic moiety and its $H_{ortho}$ center. In $TS_F$ (F = $\mathbf{III_S}$), this latter interaction may allow for rotational relaxation of the $CF_3$ group adjacent to the $H_{ortho}$ atom and therefore increase the activation entropy ($\Delta S^*_{inv} = +0.1 \pm 1.1$ cal K$^{-1}$ mol$^{-1}$).
[30] An example of lack of simultaneous validity of the compensation model and linear free-energy relationships can be found in: C. Karunakaran, P. N. Palanisamy, *Int. J. Chem. Kinet.* **1999**, *31*, 571.

Received: February 14, 2003
Revised: May 9, , 2003 [F4850]